

Microscopic theory of the Coulomb based exchange coupling in magnetic tunnel junctions

O. G. Udalov^{1,2} and I. S. Beloborodov¹

¹*Department of Physics and Astronomy, California State University Northridge, Northridge, CA 91330, USA*

²*Institute for Physics of Microstructures, Russian Academy of Science, Nizhny Novgorod, 603950, Russia*

(Dated: December 9, 2024)

We study interlayer exchange coupling (IEC) based on the many-body Coulomb interaction between conduction electrons in magnetic tunnel junction (MTJ). This mechanism complements the known IEC based on virtual electron hopping (or spin currents). We find that these two mechanisms have different behavior on system parameters. The Coulomb based IEC may exceed the hopping based exchange coupling. We show that the Coulomb based exchange coupling, in contrast to the hopping based coupling, depends strongly on the dielectric constant of the insulating layer. The dependence of the IEC on the dielectric properties of the insulating layer in MTJ is similar to magneto-electric (ME) effect where electric and magnetic degrees of freedom are coupled. We calculate the IEC as a function of temperature and electric field for MTJ with ferroelectric (FE) layer and show that IEC has a sharp decrease in the vicinity of the FE phase transition and varies strongly with external electric field.

I. INTRODUCTION

Magnetic tunnel junctions (MTJ) are of great importance these days because of their promise for next generation memory cells [1–6]. However, there are several issues to create such memory cells. One of them is control of magnetic state of ferromagnetic (FM) leads in MTJ. This problem requires a fundamental research and understanding of spin currents and interlayer exchange coupling (IEC) mechanisms in MTJ. The IEC was studied theoretically [7–15] and experimentally [12, 16–22] in numerous papers. These works show that there are several phenomena responsible for magnetic coupling between FM layers in MTJ. A weak FM coupling appears due to magneto-dipole (MD) interaction between correlated roughness in MTJ interfaces (orange peel effect) [23 and 24]. Spin currents across the insulating barrier in MTJ produce the hopping based exchange interaction [7–9] leading to the FM or antiferromagnetic (AFM) coupling depending on the system parameters [17 and 18]. In addition, the IEC was studied for insulating layer with impurities [10, 12, and 25]. In this case it gives the AFM contribution to the total magnetic coupling between FM leads. In this paper we propose a different mechanism of IEC in MTJ based on many-body Coulomb interaction.

The hopping based IEC in MTJ was studied both analytically [7–10, 13, and 15] and using the *ab initio* calculations [11, 12, and 14]. To derive the IEC the single particle Hamiltonian was used with kinetic term and the spin-dependent single-particle potential. The many-body interaction was not taken into account when calculating the IEC.

However, the exchange interaction also exists due to many-particle interaction, for example due to the Coulomb interaction. The indirect Coulomb interaction (exchange) between electrons localized at different atoms is responsible for FM and AFM states in magnetic insulators [26]. The indirect Coulomb interaction between

conduction and localized electrons in FM metals results in spin subband splitting of the conduction band [26]. In this paper we study the IEC based on the inter-electron Coulomb interaction between two FM metallic leads separated by the insulating layer.

The basic idea behind this mechanism is related to the fact that the wave functions of electrons located at different FM leads are overlapped inside the insulating layer. Since the screening effects inside the insulator are weak the long-range Coulomb interaction between these electrons exists and it has the spin-dependent part (exchange interaction) [27]. Here we study the IEC due to this indirect spin-dependent part of the Coulomb interaction and show that this contribution is comparable and even bigger than the hopping based exchange interaction.

The most important feature of the Coulomb based exchange interaction is its dependence on the dielectric permittivity of the insulating layer. This dependence can be used to distinguish this contribution from other contributions to the exchange coupling. Also this peculiarity allows to realize the magneto-electric (ME) coupling [28 and 29] in MTJ with ferroelectric (FE) insulating barrier.

The paper is organized as follows. In Sec. II we introduce the model for MTJ. In Secs. IV and V we calculate the inter-electron Coulomb interaction and the IEC in the system. We discuss and compare the Coulomb and the hopping based IEC in Sec. VI. We consider ME coupling in MTJ with FE barrier in Sec. VI. Finally, we discuss validity of our theory in Sec. VII.

II. THE MODEL

We consider two identical FM leads separated by the insulating layer of thickness d (Fig. 1). The FM leads have thickness much larger than all other characteristic length scales in the problem. We find magnetic interaction between the leads assuming that s electrons are

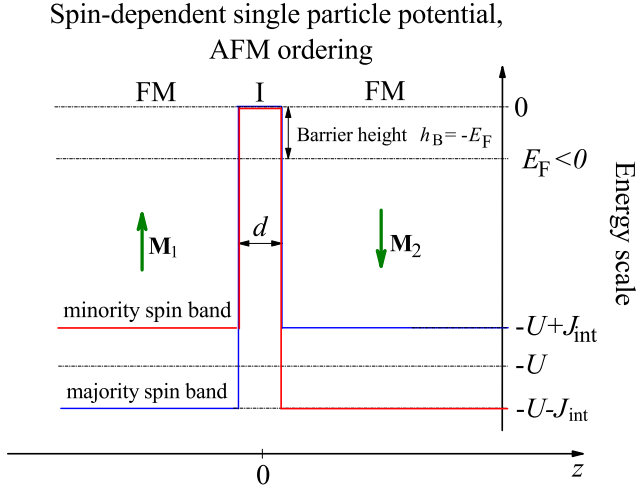


FIG. 1. (Color online) Schematic picture of potential energy profiles for electron with spin “up” and “down” states for AFM configuration of leads magnetic moments $M_{1,2}$. Zero energy corresponds to the top of energy barrier for electrons in the insulator. Symbols FM and I stand for FM metal and insulator, respectively. All other notations are defined in the text.

responsible for magnetic interaction. We assume that magneto-dipole interaction between the leads is absent. The Hamiltonian describing delocalized electrons in the system has the form

$$\hat{H} = \hat{H}_0 + \hat{H}_C, \quad (1)$$

$$\hat{H}_0 = \hat{W}_k + \hat{U}_1 + \hat{U}_2 + \hat{H}_{1\text{mag}} + \hat{H}_{2\text{mag}},$$

where \hat{W}_k is the kinetic energy of electrons, operators $\hat{U}_{1,2}$ describe potential energy profile for electrons. \hat{H}_C is the Coulomb interaction between conduction s electrons; $\hat{H}_{1,2\text{mag}}$ is the exchange interaction of delocalized electrons with localized electrons. We use Vonsovskii s-d model to describe this interaction [26]. In general the s-d interaction also appears due to the Coulomb interaction, however this interaction is between delocalized s electrons and strongly localized d electrons. The average spin-dependent potential acting on the s electrons appears due to averaging over d electrons. The s-d interaction couples d and s electrons in the same lead and does not produce coupling between the leads.

The Hamiltonian \hat{H}_0 describes single particle interactions in the system of conduction electrons. It can be represented as a sum of single particle Hamiltonians $\hat{H}_0 = \sum_i \hat{H}_0^{\text{sp}}(\mathbf{r}_i)$, with $\hat{H}_0^{\text{sp}} = \hat{W}_k^{\text{sp}} + \hat{U}_1^{\text{sp}} + \hat{U}_2^{\text{sp}} + \hat{H}_{1\text{mag}}^{\text{sp}} + \hat{H}_{2\text{mag}}^{\text{sp}}$. Single particle potential energy $\hat{U}_1^{\text{sp}} = -U\Theta(-z - d/2)$ and $\hat{U}_2 = -U\Theta(z - d/2)$, where the step function $\Theta(z) = 1$, if $z > 0$ and $\Theta(z) = 0$, if $z < 0$ and the z -axis is perpendicular to the leads surfaces; $z = 0$ is the symmetry point between FM leads. We choose the zero energy level at the top of insulating barrier (see Fig. 1). This leads to negative Fermi level $E_F < 0$. We consider only FM and AFM collinear configurations of the

leads magnetizations. Therefore according to s-d model, $\hat{H}_{1,2\text{mag}}^{\text{sp}}(\mathbf{r}_i) = -J_{\text{sd}}\hat{\sigma}_z M_{1,2}\Theta(\mp z - d/2)$ (sign “-” stands for the left and “+” for the right leads, respectively), with $M_1 = 1$ and $M_2 = \pm 1$ for FM (“+”) and AFM (“-”) configurations.

The magnetic exchange interaction between FM leads described by the Hamiltonian \hat{H}_0 was considered in Refs. [8 and 9] using a different language. The magnetic interaction was considered as a result of spin currents flowing between the leads [8] or as a consequence of varying of electron energy levels density due to interference effects in the insulating layer between the leads [9]. Using perturbation theory we consider the magnetic interaction as a result of virtual electron hopping between the leads [30]. The interlead coupling in Hamiltonian \hat{H}_0 appears as a combination of s-d interaction and the kinetic energy term. The s-d interaction produces the spin polarized s electrons in each lead while the kinetic energy term couples these spin polarized electron gases in the left and the right leads.

It is known that the exchange interaction also exists due to many particle interaction. Magnetic moments of two electrons located at different sites with overlapping wave functions are coupled due to the indirect Coulomb interaction [27]. Originally this interaction was called the exchange interaction. In this manuscript we consider the spin dependent indirect Coulomb interaction between s electrons located in different leads. This interaction leads to the magnetic coupling between the leads. Thus, we consider the s-s interaction in our manuscript. The idea is the following: s electrons located in one lead create a spin dependent potential for s electrons located in a second lead. This is in contrast to the s-d interaction where d electrons in one lead act on s electrons in the same lead.

The hopping based exchange interaction due to Hamiltonian \hat{H}_0 can be estimated as follows. Electron wave functions decay exponentially inside the insulator. Therefore the hopping matrix elements between the leads depend exponentially on distance d as $e^{-\kappa_0 d}$, where $\kappa_0 = \sqrt{-2m_e E_F/\hbar^2}$. These matrix elements are small. The hopping based exchange interaction appears in the second order perturbation theory [30] producing the factor $e^{-2\kappa_0 d}$. Since the hopping based interlead exchange interaction is due to kinetic energy it has the factor $\hbar^2 \kappa_0^2 / (2m_e)$, which always enter the tunneling matrix elements. In addition, magnetic coupling between the leads is absent if electron gas inside the leads is not spin polarized (has no magnetic moment). Therefore, the interlayer coupling is proportional to the spin polarization of s-electrons, $(J_{\text{sd}}/(U + E_F))^2$. Finally, the hopping based IEC can be estimated as follows, $H_h^{\text{ex}} \sim (\hbar^2 \kappa_0^2 / 2m_e)(J_{\text{sd}}/(U + E_F))^2 e^{-2\kappa_0 d}$, in qualitative agreement with Ref. [8].

Similarly we estimate the s-s Coulomb based exchange interaction between the leads. The matrix element of the indirect Coulomb interaction contains four electron wave functions and therefore is proportional to the square of

electron wave functions overlap. The Coulomb based exchange interaction appears in the first order perturbation theory. Therefore, it is also proportional to $e^{-2\kappa_0 d}$. Similar to the hopping based coupling the Coulomb based coupling exists only if electron gas in each lead is spin-polarized producing the factor $(J_{sd}/(U + E_F))^2$. In addition, the Coulomb interaction between two electrons inside the barrier can be estimated as $e^2/(\varepsilon d)$, where ε is the insulator dielectric constant. Combining all these factors the Coulomb based exchange coupling can be estimated as follows, $H_C^{\text{ex}} \sim (e^2/\varepsilon d)(J_{sd}/(U + E_F))^2 e^{-2\kappa_0 d}$.

For interlayer distance $d = 1$ nm, barrier height $h_B = -E_F = 0.2$ eV, and $\varepsilon = 5$ the hopping and the Coulomb based exchange contributions are comparable. Therefore the Coulomb based exchange coupling is important and should be taken into account in this problem.

We introduce Hamiltonians $\hat{H}_{1,2}$ describing a single lead with infinite insulator

$$\hat{H}_{1,2}^{\text{sp}} = \hat{W}_k^{\text{sp}} + \hat{U}_{1,2}^{\text{sp}} + \hat{H}_{1,2\text{mag}}^{\text{sp}}. \quad (2)$$

The eigenfunctions of the Hamiltonians are ψ_i^s and ϕ_i^s for leads (1) and (2), respectively. The subscript i stands for orbital state and the superscript s denotes the spin state in the local spin coordinate system related to magnetization in the corresponding lead. The wave functions are symmetric due to symmetry of the problem

$$\psi_i^s(x, y, z) = \phi_i^s(x, y, -z). \quad (3)$$

Energies of these states are ϵ_{1i}^s and ϵ_{2i}^s . For identical leads the energies are equal, $\epsilon_{1i}^s = \epsilon_{2i}^s = \epsilon_i^s$, however $\epsilon_i^s \neq \epsilon_i^{-s}$. The creation and annihilation operators in the lead (1) and (2) are \hat{a}_i^{s+} and \hat{a}_i^s , and \hat{b}_i^{s+} and \hat{b}_i^s , respectively.

We introduce the zero-order many-particle wave functions Ψ_0^{AFM} and Ψ_0^{FM} for AFM and FM configurations of leads magnetic moments $\mathbf{M}_{1,2}$. These wave functions describe the non-interacting FM layers ($d \rightarrow \infty$). All states ψ_i^s and ϕ_j^s with energies $\epsilon_i^s < E_F$ are filled and all states above E_F are empty.

Below we calculate the surface exchange interaction between the FM leads, $H^{\text{ex}} = (E^{\text{AFM}} - E^{\text{FM}})/S$, where E^{AFM} (E^{FM}) is the energy of AFM (FM) state and S is the surface area of the leads. We will assume that the insulator between the leads is thick enough and the interlayer coupling is weak and can be considered within the perturbation theory. The exchange interaction has two contributions: 1) the hopping based exchange interaction, $H_{\text{SI}}^{\text{ex}}$ - due to the Hamiltonian \hat{H}_0 and 2) the Coulomb based exchange interaction, H_C^{ex} - due to the Hamiltonian \hat{H}_C . The first contribution was studied in Ref. [8]. The second contribution is calculated in this paper. Corrections to the ground state Ψ_0 due to electron tunneling between the leads are of the order of $e^{-\kappa_0 d}$ and can be neglected in calculating the Coulomb based exchange interaction. Finally, we use the first order perturbation theory to calculate the indirect Coulomb interaction

$$H_C^{\text{ex}} = \frac{1}{S} (\langle \Psi_0^{\text{AFM}} | \hat{H}_C | \Psi_0^{\text{AFM}} \rangle - \langle \Psi_0^{\text{FM}} | \hat{H}_C | \Psi_0^{\text{FM}} \rangle). \quad (4)$$

We consider Eq. (4) in the next sections.

III. MAIN RESULTS

Our main findings are the following:

1) We calculate the exchange coupling in MTJ due to Coulomb interaction between s electrons located at different leads. We show that the Coulomb based IEC can exceed the hopping based exchange contribution studied by Slonczewski, Bruno and Jullier in the past. We find that these two mechanisms have essentially different dependence on system parameters (see Figs. 2, 3, 4, 5, 6).

2) We find that the hopping and the Coulomb based exchange interaction have the same small factor due to weak wave functions overlap, $e^{-2\kappa_0 d}$. In addition, both contributions have similar dependence on the s-d coupling constant. For small spin subband splitting both contributions are proportional to $(J_{sd}/(U + E_F))^2$. The hopping based IEC is related to the kinetic energy term in the system Hamiltonian and therefore has the factor $\hbar^2 \kappa_0^2 / (2m_e)$. The Coulomb based exchange contribution is due to electric forces acting between s-electrons, as a result it has the factor $e^2/(\varepsilon d)$.

3) We find the approximate analytical expressions for the Coulomb (H_C^{ex}) and the hopping ($H_{\text{SI}}^{\text{ex}}$) based IEC per unit area in the limit $J_{sd} \ll (U + E_F)$, $\kappa_0 \ll k_F$ ($k_F = \sqrt{2m_e(U + E_F)/\hbar^2}$)

$$H_{\text{SI}}^{\text{ex}} \approx \frac{2\hbar^2}{\pi^2 m_e d^2} \frac{J_{sd}^2}{(U + E_F)^2} \frac{\kappa_0^5}{k_F^3} e^{-2\kappa_0 d}, \quad (5)$$

$$H_C^{\text{ex}} \approx \frac{\zeta e^2}{4\pi \varepsilon_0 \varepsilon d} \frac{J_{sd}^2}{(U + E_F)^2} \frac{k_F}{d} e^{-2\kappa_0 d}, \quad (6)$$

where $\zeta \approx 1/150$.

4) We show that in contrast to hopping based exchange interaction, the Coulomb based exchange is inversely proportional to the dielectric constant ε of the insulating layer (see Fig. 7).

5) We calculate the IEC as a function of temperature and electric field (or voltage across the MTJ) for MTJ with insulating layer made of TTF-CA and $\text{Hf}_{0.5}\text{Zr}_{0.5}\text{O}_2$ (see Figs. 8, 9). We show that in the vicinity of the FE phase transition of TTF-CA the IEC has large variations. We find that even the FM-AFM transition may occur in MTJ for some system parameters.

6) We find that IEC as a function of electric field (or applied voltage) shows strong variations. The electric field can cause the transition from AFM to FM coupling: for zero field the coupling is AFM while for finite field it is FM. This effect demonstrates the ME coupling in MTJ.

IV. BASIC WAVE FUNCTIONS

We use the coordinate system with z -axis being perpendicular to the leads surfaces and x and y being per-

pendicular to z , $r_{\perp} = \sqrt{x^2 + y^2}$. In the absence of spin-orbit interaction the spin and the spatial parts of wave functions are decoupled. The spin parts are $(1\ 0)^T$ and $(0\ 1)^T$ for the spin up and spin down states, respectively. The spatial part of electron wave functions inside the leads consists of two plane waves: one going toward the leads surface and the other being reflected from the FM/insulator interface

$$\begin{aligned}\psi_i^s(z, \mathbf{r}_{\perp}) &= \frac{e^{ik_z(\frac{d}{2}+z)} + \xi_{\mathbf{k}}^s e^{-ik_z(\frac{d}{2}+z)}}{\sqrt{\Omega}} e^{i\mathbf{k}_{\perp}\mathbf{r}_{\perp}}, \quad z < -d/2 \\ \phi_i^s(z, \mathbf{r}_{\perp}) &= \frac{e^{ik_z(\frac{d}{2}-z)} + \xi_{\mathbf{k}}^s e^{-ik_z(\frac{d}{2}-z)}}{\sqrt{\Omega}} e^{i\mathbf{k}_{\perp}\mathbf{r}_{\perp}}, \quad z > d/2,\end{aligned}\quad (7)$$

where $\xi_{\mathbf{k}}^s = \frac{k_z - i\kappa_{\mathbf{k}}^s}{k_z + i\kappa_{\mathbf{k}}^s}$ is the amplitude of the reflected electron wave, with $\kappa_{\mathbf{k}}^s = \sqrt{2m_e(U - sJ_{\text{sd}})/\hbar^2 - k_z^2}$. Superscript i denotes the full set of quantum numbers (k_x, k_y, k_z) , $\mathbf{k}_{\perp} = (k_x, k_y, 0)$ and $\mathbf{r}_{\perp} = (x, y, 0)$ and Ω is the volume of each lead.

Outside the left lead we have

$$\psi_i^s(z, r_{\perp}) = \frac{\tau_{\mathbf{k}}^s}{\sqrt{\Omega}} \exp^{-\kappa_{\mathbf{k}}^s(\frac{d}{2}+z)} e^{i\mathbf{k}_{\perp}\mathbf{r}_{\perp}}, \quad z > -d/2, \quad (8)$$

where $\tau_{\mathbf{k}}^s = \frac{2k_z}{k_z + i\kappa_{\mathbf{k}}^s}$ is the amplitude of the transmitted electron wave. Outside the right lead we have

$$\psi_i^s(z, r_{\perp}) = \frac{\tau_{\mathbf{k}}^s}{\sqrt{\Omega}} \exp^{-\kappa_{\mathbf{k}}^s(\frac{d}{2}+z)} e^{i\mathbf{k}_{\perp}\mathbf{r}_{\perp}}, \quad z < d/2. \quad (9)$$

V. EXCHANGE DUE TO COULOMB INTERACTION

Both terms in Eq. (4) have contributions from direct and indirect Coulomb interaction. The direct Coulomb interaction does not lead to spin-dependent correction to the system energy and will be omitted below. Also we will omit the indirect Coulomb interaction between conduction electrons in the same lead. On one hand this contribution does not lead to interaction between the leads and on the other hand it leads to spin subband splitting which is much smaller than the splitting due to the s-d interaction.

We assume that IEC is small due to large distance between the leads and weak overlap of electron wave functions. Therefore we use the first order perturbation theory to study this coupling. We average the Coulomb operator, \hat{H}_C , over the ground state of unperturbed (non-interacting) system. We use the local coordinate spin system with z-axis being co-directed with lead magnetic moment. Therefore, the operator of Coulomb interaction is different for FM and AFM orientations of leads magnetic moments. The reduced Hamiltonian takes into account only interaction between electrons at different

leads and has the form³¹

$$\hat{H}_C^{\text{ex}} = \begin{cases} -\sum_{i,j,s} U_{ijj}^{ss} \hat{a}_i^{s+} \hat{a}_i^s \hat{b}_j^{s+} \hat{b}_j^s, & \text{FM ordering,} \\ -\sum_{i,j,s} \tilde{U}_{ijj}^{ss} \hat{a}_i^{s+} \hat{a}_i^s \hat{b}_j^{-s+} \hat{b}_j^{-s}, & \text{AFM ordering,} \end{cases} \quad (10)$$

The electron wave function has a random phase due to scattering on impurities therefore only the diagonal matrix elements of exchange interaction contribute to the system energy, $U_{ikk}^{s1s2} \neq 0$. Below we will omit the double subscripts and superscripts for matrix elements of the Coulomb interaction. The matrix element has the form [27]

$$\begin{aligned}U_{ij}^s &= \frac{1}{S} \iint d^3\mathbf{r}_1 d^3\mathbf{r}_2 \psi_i^{s*}(\mathbf{r}_1) \phi_j^s(\mathbf{r}_1) \hat{U}_C \psi_i^s(\mathbf{r}_2) \phi_j^{s*}(\mathbf{r}_2), \\ \tilde{U}_{ij}^s &= \frac{1}{S} \iint d^3\mathbf{r}_1 d^3\mathbf{r}_2 \psi_i^{s*}(\mathbf{r}_1) \phi_j^{-s}(\mathbf{r}_1) \hat{U}_C \psi_i^s(\mathbf{r}_2) \phi_j^{-s*}(\mathbf{r}_2),\end{aligned}\quad (11)$$

where \hat{U}_C is the operator of the Coulomb interaction. For homogeneous insulator it has the form $\hat{U}_C = e^2/(4\pi\epsilon_0\epsilon|\mathbf{r}_1 - \mathbf{r}_2|)$, where ϵ is the medium effective dielectric constant. In our case the system is inhomogeneous and the Coulomb interaction is renormalized by the screening effects due to metallic leads.

The right hand side of Eq. (11) can be considered as the Coulomb interaction between two effective charges, $\rho_{ij}^{(1)} = e\psi_i^{s*}(\mathbf{r})\phi_j^s(\mathbf{r})$ and $\rho_{ij}^{(2)} = e\psi_i^s(\mathbf{r})\phi_j^{s*}(\mathbf{r})$. These charges have the form

$$\begin{aligned}\rho_{ij}^{(2)*} &= \rho_{ij}^{(1)} = \frac{e\tau_i^{s*}\tau_j^{s'}}{\Omega} e^{-z(\kappa_i^s - \kappa_j^{s'})} e^{-\frac{d}{2}(\kappa_i^s + \kappa_j^{s'})} \times \\ &\quad \times e^{i(\mathbf{k}_{i\perp} - \mathbf{k}_{j\perp})\mathbf{r}_{\perp}}.\end{aligned}\quad (12)$$

Here we use $s' = s$ for FM and $s' = -s$ for AFM configurations.

The wave functions of two electrons located at different leads ψ_i and ϕ_j are overlapped inside the insulating layer and inside the leads. Therefore, there are two regions contributing to Eq. (11): 1) The region inside the FM leads Ω_1 (Ω_2) where the Coulomb interaction is effectively screened and is short-range [32]

$$\hat{U}_C^L = \frac{\Omega\Delta}{2} \delta(\mathbf{r}_1 - \mathbf{r}_2), \quad (13)$$

where Δ is the mean energy level spacing, $\Omega\Delta = 6\pi^2 E_F / ((k_F^+)^3 + (k_F^-)^3)$, with the Fermi momentum $k_F^s = \sqrt{2m_e(U + E_F - sJ_{\text{sd}})/\hbar^2}$. The peculiarity of this term is related to the fact that it does not depend on dielectric properties of insulating layer. This region gives the following contribution

$$L_{ij}^s = \frac{1}{S} \iint_{\Omega_1 + \Omega_2} d^3\mathbf{r}_1 d^3\mathbf{r}_2 \psi_i^{s*}(\mathbf{r}_1) \phi_j^s(\mathbf{r}_1) \hat{U}_C^L \psi_i^s(\mathbf{r}_2) \phi_j^{s*}(\mathbf{r}_2), \quad (14)$$

where $\Omega_{1,2} = \Omega$ is the lead volume.

2) The second region contributing to Eq. (11) is the region between the leads where screening of the Coulomb interaction is weak and the interaction is long-range. However, due to metallic leads, the electric field of two interacting electrons is finite only inside this region. We denote the renormalized Coulomb interaction inside the insulating layer as \hat{U}_C^I . This contribution depends on the dielectric permittivity ε of the insulating layer. This region produce the following contribution

$$I_{ij}^s = \frac{1}{S} \int \int_{\Omega_I} d^3\mathbf{r}_1 d^3\mathbf{r}_2 \psi_i^{s*}(\mathbf{r}_1) \phi_j^s(\mathbf{r}_1) \hat{U}_C^I \psi_i^s(\mathbf{r}_2) \phi_j^{s*}(\mathbf{r}_2), \quad (15)$$

where Ω_I is the volume of the insulating layer. We can write the matrix elements of the indirect Coulomb interaction as a sum of two terms. For FM ordering we have

$$U_{ij}^s = L_{ij}^s + I_{ij}^s, \quad (16)$$

Note that electrons inside the insulator and electrons inside the leads are decoupled and do not interact with each other.

Similarly we can write the matrix elements for AFM state \tilde{U}_{ij}^s . We can split the total IEC based on the Coulomb interaction into two contributions

$$H_C^{\text{ex}} = L^{\text{ex}} + I^{\text{ex}}. \quad (17)$$

Below we consider these two contributions to the Coulomb based exchange interaction separately.

A. Contribution to the exchange interaction due to the insulating region, I^{ex}

This contribution includes three terms: 1) \tilde{I}_{ex}^- - FM configuration, majority spin subband; 2) \tilde{I}_{ex}^+ - FM configuration, minority spin subband; \tilde{I}_{ex}^- - FM configuration, majority spin subband; 3) \tilde{I}_{ex}^- - AFM configuration (both spin subbands give the same contribution in AFM case).

Consider the first term \tilde{I}_{ex}^- . Replacing summation in Eq. (10) with integration we have

$$\tilde{I}_{\text{ex}}^- = -\frac{\Omega^2}{(2\pi)^6 S} \int \int_{\varepsilon_1^-, \varepsilon_2^- < E_F} d^3k_1 d^3k_2 I_{\mathbf{k}_1 \mathbf{k}_2}^-, \quad (18)$$

where $\varepsilon^s = \hbar^2 k^2 / (2m_e) + s J_{\text{sd}} + U$. Substituting Eq. (12) into Eq. (18) we obtain

$$\begin{aligned} \tilde{I}_{\text{ex}}^- &= \frac{-\Omega^2}{(2\pi)^6 S} \int d^3r_1 d^3r_2 d^3k_1 d^3k_2 \hat{U}_C^I(\mathbf{r}_1, \mathbf{r}_2) \times \\ &\times \tilde{\rho}(z_1) (\tilde{\rho}(z_2))^* e^{i(\mathbf{k}_{1\perp} - \mathbf{k}_{2\perp}) \cdot \mathbf{r}_{1\perp}} e^{-i(\mathbf{k}_{1\perp} - \mathbf{k}_{2\perp}) \cdot \mathbf{r}_{2\perp}}, \end{aligned} \quad (19)$$

where

$$\tilde{\rho}(z) = \frac{e\tau_i^{s*} \tau_j^s}{\Omega} e^{-z(\varkappa_i^s - \varkappa_j^s)} e^{-\frac{d}{2}(\varkappa_i^s + \varkappa_j^s)}. \quad (20)$$

The integral over $\mathbf{r}_{1,2}$ describes the interaction energy of two effective charges. According to Eq. (12) the effective charges decay exponentially along z direction and harmonically vary in the transverse direction. The effective charges produce an electric field. This field is screened by metallic leads and is finite only inside the insulating layer. The details of calculations are shown in Appendix. The final result for \tilde{I}_{ex}^- has the form

$$\begin{aligned} \tilde{I}_{\text{ex}}^- &= -\frac{e^2}{32\pi^4 \varepsilon_0 \varepsilon} \int_0^{k_F^-} \int_0^{k_1} dk_1 dk_2 |(\tau_1^-)^* \tau_2^-|^2 e^{-d(\varkappa_1^- + \varkappa_2^-)} \times \\ &\times \int_0^{k_2^{\text{max}} + k_1^{\text{max}}} q \omega_I(q) dq \int_0^{(k_2^{\text{max}} + k_1^{\text{max}})/2} k \zeta(k, q) dk, \end{aligned} \quad (21)$$

where \varkappa in the expression for $\omega_I(q)$ is taken for majority ($s = "-"$) spin subband and we introduce the notation $k_1^{\text{max}} = \sqrt{(k_F^-)^2 - k_{1z}^2}$ and $k_2^{\text{max}} = \sqrt{(k_F^-)^2 - k_{2z}^2}$. The functions $\omega_I(q)$ and $\zeta(k, q)$ are defined in Appendix.

The contribution from the minority ($s = "+"$) spin subband has the form

$$\begin{aligned} \tilde{I}_{\text{ex}}^+ &= -\frac{e^2}{32\pi^4 \varepsilon_0 \varepsilon} \int_0^{k_F^+} \int_0^{k_1} dk_1 dk_2 |(\tau_1^+)^* \tau_2^+|^2 e^{-d(\varkappa_1^+ + \varkappa_2^+)} \times \\ &\times \int_0^{k_2^{\text{max}} + k_1^{\text{max}}} q \omega_I(q) dq \int_0^{(k_2^{\text{max}} + k_1^{\text{max}})/2} k \zeta(k, q) dk. \end{aligned} \quad (22)$$

We use \varkappa for minority spin subband in the expression for $\omega_I(q)$ and $k_{1,2}^{\text{max}}$ should be taken for minority spin subband ($k_F^- \rightarrow k_F^+$).

Similarly we calculate the contribution due to AFM configuration in Eq. (4)

$$\begin{aligned} \tilde{\tilde{I}}_{\text{ex}} &= -\frac{e^2}{32\pi^4 \varepsilon_0 \varepsilon} \int_0^{k_F^+} \int_0^{k_F^-} dk_1 dk_2 |(\tau_1^+)^* \tau_2^-|^2 e^{-d(\varkappa_1^+ + \varkappa_2^-)} \times \\ &\times \int_0^{k_2^{\text{max}} + k_1^{\text{max}}} q \omega_I(q) dq \int_0^{(k_2^{\text{max}} + k_1^{\text{max}})/2} k \zeta(k, q) dk. \end{aligned} \quad (23)$$

Here we use \varkappa_2 for majority spin subband and \varkappa_1 for minority spin subband in the expression for ω_I . Similarly, we have $k_1^{\text{max}} = \sqrt{(k_F^+)^2 - k_{1z}^2}$ and $k_2^{\text{max}} = \sqrt{(k_F^-)^2 - k_{2z}^2}$. The contributions to energy of AFM configuration from both spin subband are equal and were included into $\tilde{\tilde{I}}_{\text{ex}}$. Using Eqs. (A17) and (23) we find the total contribution to the exchange interaction due to the insulating region

$$I^{\text{ex}} = \tilde{\tilde{I}}_{\text{ex}} - \tilde{I}_{\text{ex}}^+ - \tilde{I}_{\text{ex}}^-. \quad (24)$$

B. Contribution to the exchange interaction due to the FM leads, L^{ex}

In metallic leads the Coulomb interaction is short-range therefore the matrix element of the exchange in-

teraction has the form

$$L_{ij}^s = \frac{\Omega\Delta}{2S} \int_{\Omega_1+\Omega_2} d^3\mathbf{r} |\psi_i^s(\mathbf{r})|^2 |\phi_j^{s'}(\mathbf{r})|^2, \quad (25)$$

where $s' = s$ for FM and $s' = -s$ for AFM states. Using Eqs. (7) and (8) we obtain for normalized matrix element the following result

$$L_{ij}^s = \frac{\Delta|\tau_j^s|^2 e^{-2d\chi_j^s}}{\Omega} \left(\frac{1 + |r_i^{s'}|^2}{2\chi_j^s} + \text{Re} \left(\frac{(r_i^{s'})^*}{\chi_j^s + ik_i} \right) \right) + \frac{\Delta|\tau_i^{s'}|^2 e^{-2d\chi_i^{s'}}}{\Omega} \left(\frac{1 + |r_j^s|^2}{2\chi_i^{s'}} + \text{Re} \left(\frac{(r_j^s)^*}{\chi_i^{s'} + ik_j} \right) \right), \quad (26)$$

Integrating this matrix elements over all eigenstates of the ground state we find for FM configuration

$$\begin{aligned} \tilde{L}_{\text{ex}}^s &= \frac{3(U + E_F)}{2^6\pi((k_F^+)^3 + (k_F^-)^3)} \times \\ &\times \int_0^{k_F^s} dk_1 \int_0^{k_F^s} dk_2 ((k_F^s)^2 - k_2^2)((k_F^s)^2 - k_1^2) \times \\ &\times \left\{ e^{-2d\chi_1^s} |\tau_1^s|^2 \left(\frac{1 + |r_2^s|^2}{2\chi_1^s} + \text{Re} \left(\frac{(r_2^s)^*}{\chi_1^s + ik_2} \right) \right) + \right. \\ &\left. |r_2^s|^2 e^{-2d\chi_2^s} \left(\frac{1 + |r_1^s|^2}{2\chi_2^s} + \text{Re} \left(\frac{(r_1^s)^*}{\chi_2^s + ik_1} \right) \right) \right\}, \quad (27) \end{aligned}$$

and for AFM configuration we have

$$\begin{aligned} \tilde{\tilde{L}}_{\text{ex}} &= \frac{6(U + E_F)}{2^6\pi((k_F^+)^3 + (k_F^-)^3)} \times \\ &\times \int_0^{k_F^+} dk_1 \int_0^{k_F^-} dk_2 ((k_F^-)^2 - k_2^2)((k_F^+)^2 - k_1^2) \times \\ &\times \left\{ e^{-2d\chi_1^+} |\tau_1^+|^2 \left(\frac{1 + |r_2^-|^2}{2\chi_1^+} + \text{Re} \left(\frac{(r_2^-)^*}{\chi_1^+ + ik_2} \right) \right) + \right. \\ &\left. |r_2^-|^2 e^{-2d\chi_2^-} \left(\frac{1 + |r_1^+|^2}{2\chi_2^-} + \text{Re} \left(\frac{(r_1^+)^*}{\chi_2^- + ik_1} \right) \right) \right\}. \quad (28) \end{aligned}$$

Using Eqs. (27) and (28) we find the total contribution to the exchange interaction due to the leads

$$L^{\text{ex}} = \tilde{\tilde{L}}_{\text{ex}} - \tilde{L}_{\text{ex}}^+ - \tilde{L}_{\text{ex}}^-. \quad (29)$$

C. Total exchange interaction

The total exchange interaction is given by the expression

$$H^{\text{ex}} = H_{\text{Sl}}^{\text{ex}} + \tilde{\tilde{L}}_{\text{ex}} - \tilde{L}_{\text{ex}}^+ - \tilde{L}_{\text{ex}}^- + \tilde{\tilde{L}}_{\text{ex}} - \tilde{L}_{\text{ex}}^+ - \tilde{L}_{\text{ex}}^-. \quad (30)$$

The first term was calculated in Ref. [8]

$$H_{\text{Sl}}^{\text{ex}} = \frac{\hbar^2}{\pi^2 m_e d^2} \chi_0^5 b e^{-2\chi_0 d},$$

$$b = \begin{cases} \frac{(\chi_0^2 - k_F^+ k_F^-)(k_F^+ - k_F^-)^2 (k_F^+ + k_F^-)}{(\chi_0^2 + (k_F^+)^2)^2 (\chi_0^2 + (k_F^-)^2)^2}, & U + E_F > J_{\text{sd}}, \\ \frac{k_F^- ((k_F^-)^2 + i\chi_0 k_F^+)}{\chi_0 (\chi_0^2 + (k_F^-)^2) (\chi_0 - ik_F^+)}, & U + E_F < J_{\text{sd}}. \end{cases} \quad (31)$$

Here the coefficient b is always real. For $U + E_F < J_{\text{sd}}$ (the second line) the Fermi momentum k_F^+ is imaginary, $k_F^+ = i|k_F^+|$.

D. Half metals

For half metals with one spin subband ($U + E_F < J_{\text{sd}}$) the first contribution in Eq. (4) is absent and only the majority spin subband contributes to the second term in Eq. (4).

E. Analytical expression for limiting case

For weak spin subband splitting, $J_{\text{sd}} \ll (U + E_F)$ and large decay length, $\chi_0 \ll k_F$, the IEC is quadratic in J_{sd} and can be written in powers of small parameter χ_0/k_F . In the leading order we find

$$H_{\text{Sl}}^{\text{ex}} \approx \frac{2\hbar^2}{\pi^2 m_e d^2} \frac{J_{\text{sd}}^2}{(U + E_F)^2} \frac{\chi_0^5}{k_F^3} e^{-2\chi_0 d}, \quad (32)$$

and for the Coulomb based IEC

$$H_C^{\text{ex}} \approx \frac{\zeta e^2}{4\pi\epsilon_0\epsilon d} \frac{J_{\text{sd}}^2}{(U + E_F)^2} \frac{k_F}{d} e^{-2\chi_0 d}, \quad (33)$$

with $\zeta \approx 1/150$. The expression for the Coulomb based IEC is derived by fitting Eq. (4). Obviously, in this limit the Coulomb based contribution dominates in the IEC.

VI. DISCUSSION OF RESULTS

A. Comparison of three contributions to the total exchange interaction

We split the total exchange interaction into three components $H_{\text{Sl}}^{\text{ex}}$, L^{ex} and I^{ex} . These contributions have different origins and behavior. The first contribution, $H_{\text{Sl}}^{\text{ex}}$, appears due to spin current between the leads. The second, L^{ex} , and the third, I^{ex} , contributions are due to many-body effects. It is important that I^{ex} depends on the dielectric permittivity of the insulating layer in contrast to the first and the second contributions.

Figure 2 shows the dependence of three contributions on the barrier height h_B , in our notations $h_B = -E_F$, for the following parameters: $U = 5$ eV, $d = 1$ nm,

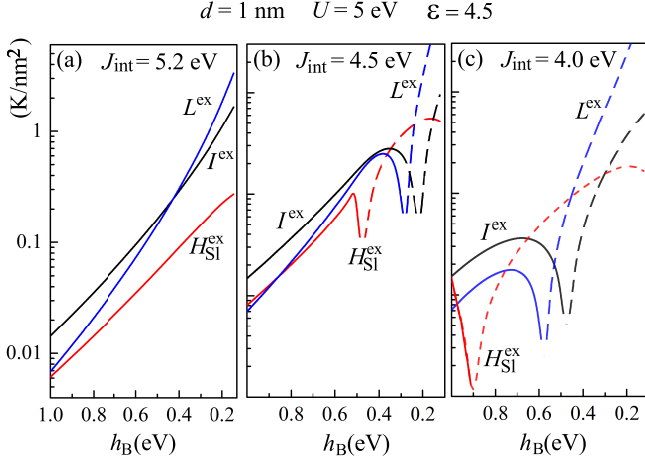


FIG. 2. (Color online) The interlayer exchange interaction as a function of insulating barrier height h_B for $U = 5 \text{ eV}$, $\varepsilon = 4.5$, $d = 1 \text{ nm}$ and (a) $J_{sd} = 5.2 \text{ eV}$, (b) $J_{sd} = 4.5 \text{ eV}$, (c) $J_{sd} = 4 \text{ eV}$. Black lines show $|I^{\text{ex}}|$ (Eq. (24)), blue lines are for $|L^{\text{ex}}|$ (Eq. (29)) and red lines are for $|H_{\text{Si}}^{\text{ex}}|$ (Eq. (31)). The y-axis has logarithmic scale. Dashed parts show the region where functions I^{ex} , L^{ex} and $H_{\text{Si}}^{\text{ex}}$ are negative.

$\varepsilon = 4.5$, $J_{sd} = 5.2; 4.5; 4.0 \text{ eV}$. All three contributions have different behavior as a function of barrier height h_B . For large spin subband splitting, J_{sd} (half metals) shown in Fig. 2(a) all three contributions are positive. For small J_{sd} (two spin subband metals) all three contributions are non-monotonic and change their sign and can be either of FM or AFM type depending on the barrier height. The contribution I^{ex} (black line) depends on the dielectric permittivity of the insulating layer in contrast to two other contributions. We use SiO_2 with $\varepsilon = 4.5$ as an example. For insulators with high dielectric constants $\varepsilon > 100$ this contribution is suppressed.

Figure 2 shows that all three contributions to the IEC are comparable and there is no a single component dominating in the whole range of parameters, especially if we take into account the fact that all three components change their sign at different values of barrier height. For strong subband splitting (half metal) and $\varepsilon < 4$ the Coulomb based contribution dominates for any barrier heights. This contribution also dominates for small spin subband splitting in the region of high barrier height ($h_B > 0.3 \text{ eV}$ for $J_{sd} = 4.5 \text{ eV}$ and $h_B > 0.6 \text{ eV}$ for $J_{sd} = 4.0 \text{ eV}$). For spin subband splitting smaller than the average conduction band width, $W_{\text{con}} = U + E_F$, and for low barrier height ($h_B < 0.3 \text{ eV}$ in Fig. 2) the Coulomb based exchange interaction, L^{ex} provides the main contribution to the IEC. For spin subband splitting smaller than the average conduction band width, W_{con} there is also a region where the hopping based exchange interaction, $H_{\text{Si}}^{\text{ex}}$ dominates. Using the fact that I^{ex} depends on the dielectric constant, in experiment one can have any relation between these three contributions.

Figure 3 shows the dependence of the total Coulomb

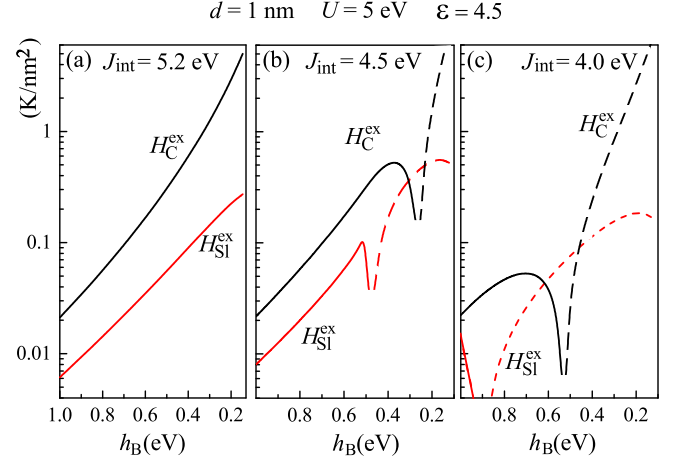


FIG. 3. (Color online) The interlayer exchange interaction as a function of h_B for $U = 5 \text{ eV}$, $\varepsilon = 4.5$, $d = 1 \text{ nm}$ and (a) $J_{sd} = 5.2 \text{ eV}$, (b) $J_{sd} = 4.5 \text{ eV}$, (c) $J_{sd} = 4 \text{ eV}$. Black lines are for $|H_C^{\text{ex}}|$ (Eq. (17)), and red lines are for $|H_{\text{Si}}^{\text{ex}}|$ (Eq. (31)). Dashed parts show the region where functions H_C^{ex} and $H_{\text{Si}}^{\text{ex}}$ are negative.

based exchange contribution, $H_C^{\text{ex}} = I^{\text{ex}} + L^{\text{ex}}$ and the hopping based contribution, $H_{\text{Si}}^{\text{ex}}$ as a function of barrier height, h_B . Both contributions have qualitatively similar behavior. For large barrier height both contributions are positive (FM) while for small barrier both contributions are negative (AFM). The FM/AFM transition point of the Coulomb based contribution is located above the transition point of the hopping based exchange. The Coulomb based exchange mostly exceeds the hopping based exchange. Only in the vicinity of the FM/AFM transition point of H_C^{ex} the hopping based exchange dominates.

Figure 4 shows the behavior of the IEC as a function of the insulator thickness d for the following parameters $U = 5 \text{ eV}$, $\varepsilon = 4.5; 15$. The Coulomb and the hopping based contributions are shown separately. The total exchange interaction is also shown. The barrier height and the spin subband splitting is different for different panels. Panel (b) ($J_{sd} = 4.5 \text{ eV}$ and $h_B = 0.6 \text{ eV}$, half-metal leads) shows the case when the Coulomb exchange dominates. In this case the exchange coupling decays exponentially with thickness d and has the same decay rate as the hopping based exchange ($e^{-2d\lambda_0}/d^2$). Therefore the dependence on thickness does not allow to distinguish the Coulomb and the hopping based exchange contributions.

Panel (c) ($J_{sd} = 2.0 \text{ eV}$ and $h_B = 1.4 \text{ eV}$, two spin subband metal) shows the opposite situation when the hopping based exchange coupling dominates. Figure 4(a) ($J_{sd} = 4 \text{ eV}$, $h_B = 0.6 \text{ eV}$) shows the case when both contributions are of the same order. In this situation the Coulomb based exchange interaction has a more complicated behavior which is substantially different from the behavior of the hopping based exchange contribution. At some thickness the Coulomb based contribution changes

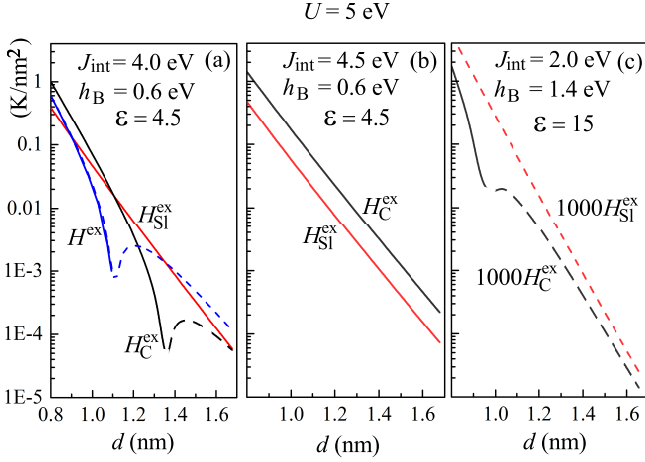


FIG. 4. (Color online) The interlayer exchange interaction as a function of the insulator thickness d for $U = 5$ eV, and (a) $J_{sd} = 4.0$ eV, $h_B = 0.6$ eV, $\varepsilon = 4.5$, (b) $J_{sd} = 4.5$ eV, $h_B = 0.6$ eV, $\varepsilon = 4.5$, (c) $J_{sd} = 2.0$ eV, $h_B = 1.4$ eV, $\varepsilon = 15$. Black lines are for $|H_C^{\text{ex}}|$ (Eq. (17)), red lines are for $|H_{\text{Sl}}^{\text{ex}}|$ (Eq. (31)), blue line is for total exchange interaction, H^{ex} (Eq. (30)). Dashed parts show the region where functions are negative.

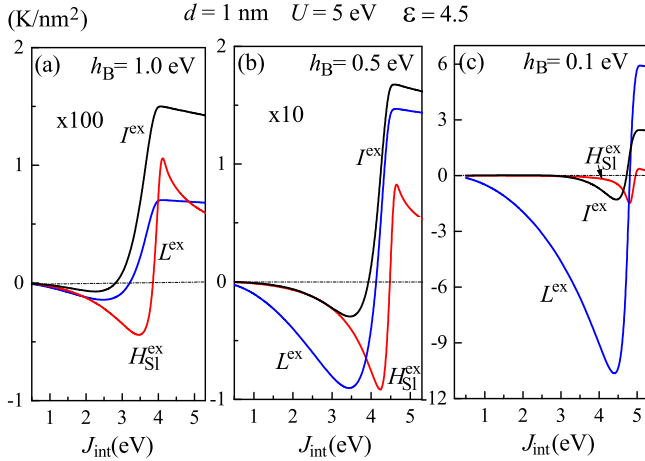


FIG. 5. (Color online) The interlayer exchange interaction as a function of spin subband splitting, J_{sd} , for $U = 5$ eV, $\varepsilon = 4.5$, $d = 1$ nm, and (a) $h_B = 1.0$ eV, (b) $h_B = 0.5$ eV, (c) $h_B = 0.1$ eV. Black lines are for I^{ex} (Eq. (24)), blue line is for L^{ex} (Eq. (29)), and red lines are for $H_{\text{Sl}}^{\text{ex}}$ (Eq. (31)). The data are multiplied by 100 in panel (a) and by 10 in panel (b).

its sign. For small thickness the Coulomb based contribution H_C^{ex} is positive (FM) while the hopping based exchange is negative (AFM). For large thickness both contributions are of AFM type. The blue curve shows the total IEC. One can see that H^{ex} also changes its sign. Such a behavior is due to competition of two contributions. The Coulomb based exchange interaction can be studied using this non-monotonic behavior.

Figure 5 shows the dependence of the exchange cou-

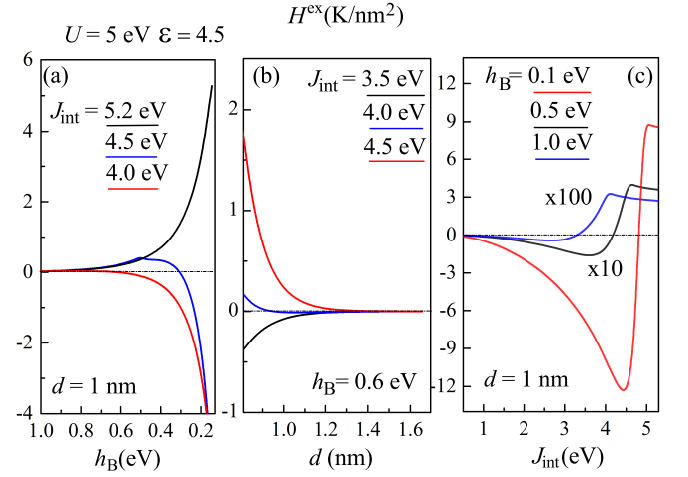


FIG. 6. (Color online) Total interlayer exchange coupling (IEC), H^{ex} in Eq. (30) as a function of (a) barrier height h_B ; (b) barrier thickness d ; (c) and the spin subband splitting J_{sd} for $U = 5$ eV, $\varepsilon = 4.5$. In panel (c) the data for $h_B = 1.0$ eV are multiplied by 100 and for $h_B = 0.5$ eV by 10.

pling on the spin subband splitting J_{sd} for $U = 5$ eV, $\varepsilon = 4.5$, $d = 1$ nm, and $h_B = 1.0; 0.5; 0.1$ eV. These plots show that contribution I^{ex} dominates if only one spin subband is filled ($J_{sd} > U + E_F$). In this region all contributions are positive (FM). For small splitting the main contribution is due to hopping, $H_{\text{Sl}}^{\text{ex}}$ and the Coulomb based, L^{ex} exchange. In the region $J_{sd} < U + E_F$ these two components are negative (AFM). Figure 5 shows that transition from FM to AFM coupling for different contributions appear at different values of the spin subband splitting, J_{sd} . In addition, the behavior of all contributions strongly depends on the barrier height.

B. Total IEC vs spin subband splitting J_{sd} , barrier height h_B and insulator thickness d

Figure 6 shows the total IEC, H^{ex} in Eq. (30) as a function of barrier height h_B , barrier thickness d , and the spin subband splitting J_{sd} for $U = 5$ eV, $\varepsilon = 4.5$. These curves show that the total IEC behaves qualitatively similar to the hopping based exchange interaction. It exponentially decays with the thickness of the insulating layer and decays with increasing the barrier height. For small spin subband splitting the coupling is weak and negative (AFM). For large subband splitting the IEC becomes FM (positive) and reaches its maximum value. The important feature of the Coulomb based exchange coupling is its dependence on the dielectric constant ε of insulator layer. The hopping based exchange coupling does not depend on ε .

C. Coulomb based exchange coupling vs dielectric permittivity of the insulating layer: ME effect

The important feature of the Coulomb based exchange interaction is its dependence on the insulator dielectric permittivity ε . The Coulomb based exchange interaction has two contributions: 1) The indirect Coulomb interaction inside the leads - L^{ex} in Eq. (29). This term does not depend on the properties of the insulating layer. 2) The indirect Coulomb interaction inside the insulating layer - I^{ex} in Eq. (24). This term is inversely proportional to the dielectric constant of the insulating layer, $I^{\text{ex}} \sim \varepsilon^{-1}$. To observe a strong dependence of the total IEC, H^{ex} , on ε the MTJ should be made of materials with large I^{ex} contribution, larger than two other contributions. Figures 2 and 5 show that the Coulomb based exchange interaction is the largest contribution for strong spin subband splitting ($J_{\text{sd}} > U + E_{\text{F}}$) and not too small barrier height. Figure 7 shows the total exchange as a function of the dielectric constant at different J_{sd} and h_{B} . These curves can be fitted using the expression

$$H^{\text{ex}} = H_0^{\text{ex}} + \frac{I_1^{\text{ex}}}{\varepsilon}, \quad (34)$$

where $H_0^{\text{ex}} = H_{\text{Sl}}^{\text{ex}} + L^{\text{ex}}$ is the part of the total exchange coupling which does not depend on the dielectric permittivity and I_1^{ex} is the Coulomb based exchange coupling inside the insulator for $\varepsilon = 1$. Note that $I_1^{\text{ex}} > 0$ is positive (FM). Depending of the barrier height h_{B} , the thickness d of the insulator, and the spin subband splitting the contribution H_0^{ex} can be either positive (green, black, blue and red curves in Fig. 7) or negative (brown curve in Fig. 7). For negative H_0^{ex} the total IEC changes its sign with increasing the dielectric permittivity of the insulating layer. For small ε the IEC is positive (FM) while for large ε it is negative (AFM). The IEC decreases more than twice with changing the permittivity ε from 5 to 50. The dependence of H^{ex} on ε can be used to distinguish this contribution from the hopping based exchange coupling. In experiment one can use an insulator with dielectric constant depending on some external parameter. In FE the dielectric permittivity depends on temperature and electric field. However, most FEs have rather large dielectric constants, $\varepsilon > 100$. These values of ε can suppress the Coulomb based exchange coupling. It is important to use FE with low dielectric permittivity such as TTF-CA [33 and 34] or $\text{Hf}_{0.5}\text{Zr}_{0.5}\text{O}_2$ [35].

Figure 8 shows behavior of IEC, H^{ex} , with TTF-CA FE as an insulating layer. The FE Curie point of TTF-CA is $T_{\text{C}} = 56$ K [36 and 37]. Using data of Refs. [36 and 37] we find the temperature dependence of TTF-CA dielectric constant. Experimental data are fitted well with the following dependence of dielectric constant on temperature

$$\varepsilon(T) = 10 + \frac{25}{1 + (T - T_{\text{C}})^2/\Delta T^2}, \quad (35)$$

where $T_{\text{C}} = 56$ K is the Curie temperature of the ferroelectric-paraelectric (FE/PE) phase transition of

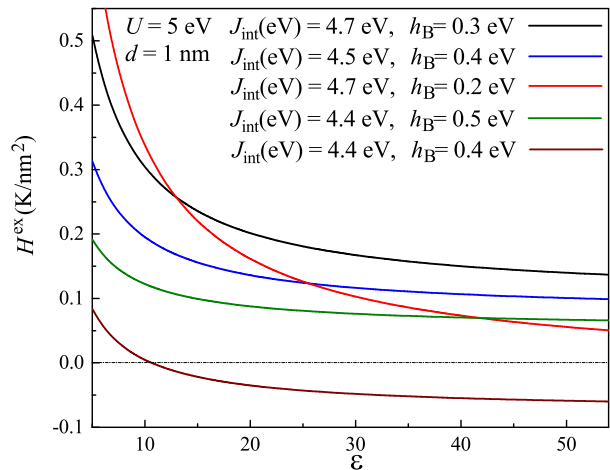


FIG. 7. (Color online) Total interlayer exchange coupling (IEC), H^{ex} in Eq. (30) as a function of dielectric permittivity of the insulating layer, ε , for $U = 5$ eV, $d = 1$ nm and different spin subband splitting, J_{sd} , and barrier height h_{B} .

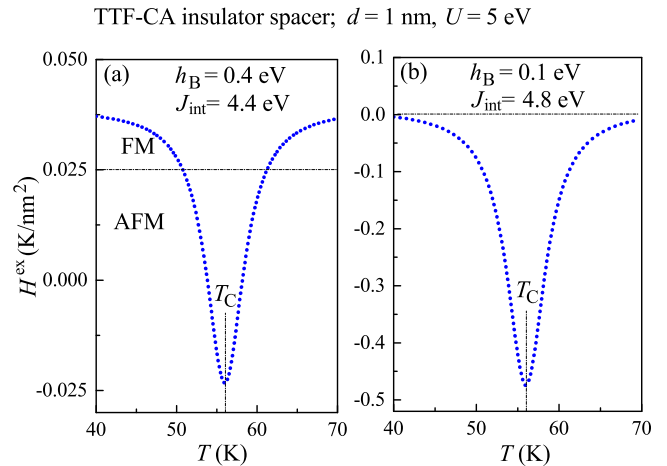


FIG. 8. (Color online) Total IEC, H^{ex} in Eq. (30) as a function of temperature for MTJ with TTF-CA FE layer (ε is given by Eq. (35)). The system parameters are: $U = 5$ eV $d = 1$ nm, and (a) $J_{\text{sd}} = 4.4$ eV, $h_{\text{B}} = 0.4$ eV; (b) $J_{\text{sd}} = 4.8$ eV, $h_{\text{B}} = 0.1$ eV. T_{C} is the TTF-CA Curie point.

TTF-CA and $\Delta T = 1.5$ K is the width of the peak. In the vicinity of the FE phase transition the dielectric permittivity of TTF-CA increases leading to decrease of the IEC. Panel (a) shows the change of sign of IEC from FM to AFM state in the vicinity of the FE/PE phase transition. Panel (b) shows the case of zero IEC away from the FE Curie point and finite IEC in the vicinity of T_{C} .

Figure 9 shows the interlayer exchange coupling, H^{ex} vs external electric field for $\text{Hf}_{0.5}\text{Zr}_{0.5}\text{O}_2$ FE layer. Here the voltage is applied across the MTJ with 1 nm $\text{Hf}_{0.5}\text{Zr}_{0.5}\text{O}_2$ insulating layer. This voltage produces an

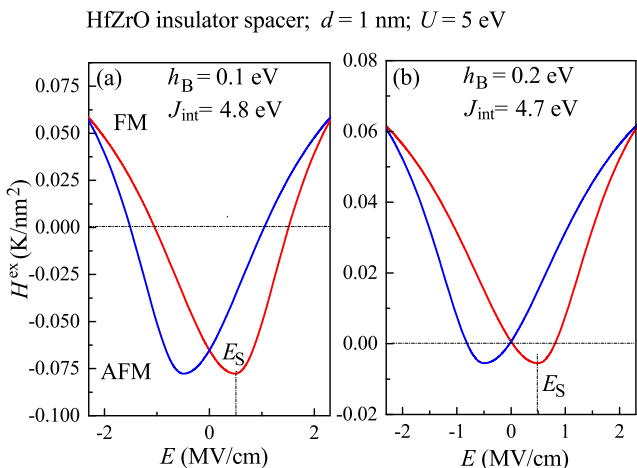


FIG. 9. (Color online) Total IEC H^{ex} Eq. (30) as a function of electric field inside of the insulating layer (voltage applied across MTJ) for MTJ with $\text{Hf}_{0.5}\text{Zr}_{0.5}\text{O}_2$ FE layer. The system parameters are: $U = 5$ eV $d = 1$ nm, and (a) $J_{\text{sd}} = 4.8$, eV $h_{\text{B}} = 0.1$ eV; (b) $J_{\text{sd}} = 4.7$, $h_{\text{B}} = 0.2$ eV. E_{S} is the FE polarization switching field.

electric field inside the FE. We use data of Ref. [35] for the dependence of dielectric constant on the electric field for $\text{Hf}_{0.5}\text{Zr}_{0.5}\text{O}_2$ FE. The curves in Fig. 9 are shown at room temperature where $\text{Hf}_{0.5}\text{Zr}_{0.5}\text{O}_2$ is in the FE phase. The dielectric permittivity ε vs electric field has two branches due to hysteresis and it has two peaks in the vicinity of the switching fields, $E = \pm E_{\text{S}}$. These two peaks correspond to two dips in the H^{ex} curves. Panel (a) shows the change of sign of IEC with applied voltage: at zero voltage the coupling is AFM while at larger voltages the crossover from AFM to FM coupling occurs. Panel (b) shows the case of zero IEC at zero electric field and finite IEC at finite electric field. Thus, this panel explicitly shows the possible to control the IEC in MTJ using electric field.

The dependence of the IEC on dielectric permittivity is due to coupling between magnetic and electrical degrees of freedom appearing due to the Coulomb nature of the magnetic exchange interaction. A similar effect was predicted semi-phenomenologically for granular magnets [38–41]. Due to this coupling between the dielectric properties of the insulating matrix and the exchange interaction the MTJ with FE layer shows the ME effect, see Fig. 9.

VII. VALIDITY OF OUR MODEL

Below we discuss several assumptions and approximations of our theory.

1) We assume that the leads are “perfect” metals meaning that they screen the electric field completely. We use this assumption to calculate the electric field in-

side the insulating layer. We assume that the field created by charges is zero inside the metal. Similarly we assume that the Coulomb interaction inside the metal is a short-range and is described by the δ -function. In fact, the electric potential created by a point charge located in a metal decays exponentially with distance, $\sim e^{-r/\lambda_{\text{TF}}}/r$, where λ_{TF} is Thomas-Fermi length. The electric field created by a charge located outside the metal also penetrates into the metal up to the distance λ_{TF} . Therefore in the vicinity of the metal surface (for distances less than λ_{TF}) our consideration is not valid. However, the Thomas-Fermi length is of the order of 0.05 nm and is much smaller than the characteristic length scales of wave function decay κ_0 and the insulator thickness d .

Also the metal-insulator barrier is not a step function as we assumed. The smearing of the boundary is comparable with λ_{TF} . In this region the classical description of screening in the insulating barrier is not valid. We use the method of image charges to calculate screening. This approach works well if the distance from the metal surface is larger than the size of exchange-correlation hole which is less than 0.1 nm. For distances less than 0.1 nm to the metal surface a quantum theory is required to describe the screening effects. Thus, our theory is not valid for MTJ with mono-layer insulating barrier [22].

2) In Sec. VI we discuss the ME coupling in MTJ due to the Coulomb based exchange interaction. To observe this coupling the FE layer should be present between magnetic leads. For strong exchange coupling the thickness of the insulating barrier should be about 1 nm. It is known that the FE Curie temperature decreases with decreasing the FE thickness [42 and 43]. Some FEs show the critical thickness where FE properties can disappear. However, there are FEs that can keep their properties down to a single atomic layer thickness [42 and 43]. In this paper we have not discussed the influence of size effects on the FE properties of insulating layer.

3) The voltage across the MTJ, necessary for creation of electric field in the insulating barrier, causes the electric and spin currents through the barrier. Such a current produces a spin transfer torque leading to magnetic interaction between FM leads. This effect was not discussed here.

4) *Ab initio* calculations based on DFT theory mostly use the local spin density (LSD) approximation treating the indirect Coulomb interaction (exchange) as the short-range interaction, $\hat{H}_{\text{C}} \sim \delta(\mathbf{r}_1 - \mathbf{r}_2)$. This approach is valid only if the characteristic scales of the electron density variations are much larger than the screening radius and the Fermi length [44 and 45]. Such an approximation works well inside the FM leads. However, inside the insulating layer the electron densities are low and the screening length exceeds the layer thickness. One can expect that the size of the exchange-correlation hole essentially exceeds the thickness of the insulating layer. In this case the Coulomb interaction is not the short range interaction any more. In this paper we take into account the long-range nature of the Coulomb interaction inside

the insulating layer. Therefore, the LSD approximation can not be used to describe effects discussed in this paper.

VIII. CONCLUSION

We studied the exchange coupling in MTJ consisting of two FM layers separated by the insulating layer. We calculated the exchange coupling due to many-body effects (the inter-electron Coulomb interaction). The basic idea behind this mechanism is related to the fact that the wave functions of electrons located at different FM leads are overlapped inside the insulating layer. In combination with weak screening of electric field inside the insulator these electrons experience the indirect Coulomb interaction leading to interlayer magnetic coupling. We showed that the Coulomb based IEC can exceed the hopping based exchange contribution and found that these two mechanisms have essentially different dependence on system parameters.

We found that, in contrast to hopping based exchange, the Coulomb based exchange interaction is inversely proportional to the dielectric constant ϵ of the insulating layer. The dependence of the IEC on the dielectric properties of the insulating layer in MTJ is similar to ME effect where electric and magnetic degrees of freedom are coupled.

We calculated the IEC as a function of temperature and electric field (or voltage across the MTJ) for MTJ with insulating layer made of TTF-CA and $\text{Hf}_{0.5}\text{Zr}_{0.5}\text{O}_2$. We showed that in the vicinity of the FE phase transition of TTF-CA the IEC experiences large variations. We found that even the FM-AFM transition may occur in MTJ for some system parameters.

We found that IEC as a function of electric field (or applied voltage) shows strong variations. The electric field can cause the transition from AFM to FM coupling: for zero field the coupling is AFM while for finite field it is FM. This effect demonstrates the ME coupling in MTJ.

IX. ACKNOWLEDGEMENTS

This research was supported by NSF under Cooperative Agreement Award EEC-1160504, the U.S. Civilian Research and Development Foundation (CRDF Global) and NSF PREM Award.

Appendix A: Contribution to the IEC from the insulating layer

Here we calculate the following integral

$$\begin{aligned} \tilde{I}_{\text{ex}}^- &= \frac{-\Omega^2}{(2\pi)^6 S} \int d^3 r_1 d^3 r_2 d^3 k_1 d^3 k_2 \hat{U}_C^1(\mathbf{r}_1, \mathbf{r}_2) \times \\ &\times \tilde{\rho}(z_1) (\tilde{\rho}(z_2))^* e^{i(\mathbf{k}_{1\perp} - \mathbf{k}_{2\perp})\mathbf{r}_{1\perp}} e^{-i(\mathbf{k}_{1\perp} - \mathbf{k}_{2\perp})\mathbf{r}_{2\perp}}. \end{aligned} \quad (\text{A1})$$

The integration over the coordinates \mathbf{r}_1 and \mathbf{r}_2 in Eq. (A1) is performed over the region between the leads. Renaming variables $\mathbf{k}_{1\perp} \rightarrow \mathbf{k}_{2\perp}$ and $\mathbf{k}_{2\perp} \rightarrow \mathbf{k}_{1\perp}$ makes the integrand complex conjugate, however the whole integral stays the same meaning that only the real part of the integral is finite. Below we consider the real part of the integrand

$$\begin{aligned} \tilde{I}_{\text{ex}}^- &= \frac{-\Omega^2}{(2\pi)^6 S} \int d^3 r_1 d^3 r_2 d^3 k_1 d^3 k_3 \times \\ &\times \tilde{\rho}(z_1) \hat{U}_C^1(\mathbf{r}_1, \mathbf{r}_2) (\tilde{\rho}(z_2))^* \times \\ &\{ \cos((\mathbf{k}_{1\perp} - \mathbf{k}_{2\perp})\mathbf{r}_1) \cos((\mathbf{k}_{1\perp} - \mathbf{k}_{2\perp})\mathbf{r}_2) + \\ &+ \sin((\mathbf{k}_{1\perp} - \mathbf{k}_{2\perp})\mathbf{r}_1) \sin((\mathbf{k}_{1\perp} - \mathbf{k}_{2\perp})\mathbf{r}_2) \}. \end{aligned} \quad (\text{A2})$$

Both terms (with $\sin()$ and $\cos()$) give the same contribution. Thus, we consider one term with numerical factor 2

$$\begin{aligned} \tilde{I}_{\text{ex}}^- &= \frac{-2\Omega^2}{(2\pi)^6 S} \int d^3 r_1 d^3 r_2 d^3 k_1 d^3 k_3 \times \\ &\times \tilde{\rho}(z_1) \hat{U}_C^1(\mathbf{r}_1, \mathbf{r}_2) (\tilde{\rho}(z_2))^* \times \\ &\times \cos((\mathbf{k}_{1\perp} - \mathbf{k}_{2\perp})\mathbf{r}_1) \cos((\mathbf{k}_{1\perp} - \mathbf{k}_{2\perp})\mathbf{r}_2). \end{aligned} \quad (\text{A3})$$

The last integral can be written in the form

$$\begin{aligned} \tilde{I}_{\text{ex}}^- &= \frac{-4\Omega^2}{(2\pi)^6 S} \int_0^{k_F^-} dk_{1z} \int_0^{k_{1z}} dk_{2z} \int d^3 r_1 d^3 r_2 \times \\ &\times \int_{|\mathbf{k}_{1\perp}|^2 < (k_F^-)^2 - k_{1z}^2} d^2 k_{1\perp} \int_{|\mathbf{k}_{2\perp}|^2 < (k_F^-)^2 - k_{2z}^2} d^2 k_{2\perp} \tilde{\rho}(z_1) (\tilde{\rho}(z_2))^* \times \\ &\times \hat{U}_C^1(\mathbf{r}_1, \mathbf{r}_2) \cos((\mathbf{k}_{1\perp} - \mathbf{k}_{2\perp})\mathbf{r}_1) \cos((\mathbf{k}_{1\perp} - \mathbf{k}_{2\perp})\mathbf{r}_2). \end{aligned} \quad (\text{A4})$$

Equation (A4) shows that the exchange interaction is the sum of matrix elements of the Coulomb interaction between the effective charges. These charges decay toward the middle of the barrier, $z = 0$, and oscillate in the (x, y) -plane. The oscillations are coherent and have the same phase.

The normalized matrix element of the effective Coulomb interaction is given by the expression

$$\begin{aligned} W_{\bar{1}} &= \frac{1}{S} \int d^3 r_1 d^3 r_2 \tilde{\rho}(z_1) (\tilde{\rho}(z_2))^* \times \\ &\times \hat{U}_C^1(\mathbf{r}_1, \mathbf{r}_2) \cos((\mathbf{k}_{1\perp} - \mathbf{k}_{2\perp})\mathbf{r}_1) \cos((\mathbf{k}_{1\perp} - \mathbf{k}_{2\perp})\mathbf{r}_2). \end{aligned} \quad (\text{A5})$$

We introduce the notations $\rho_0^2 = |e\tau_i^{s*} \tau_j^s / \Omega|^2$, $\Delta\mathcal{K} = \mathcal{K}_1 - \mathcal{K}_2$, $\mathbf{q} = \mathbf{k}_{1\perp} - \mathbf{k}_{2\perp}$ ($q = |\mathbf{q}|$). To evaluate the matrix element we calculate the electric field created by the effective charges. Due to periodic harmonic variations of the electric charge the field has the same harmonic variations. The electric field inside the metallic leads is zero since it is screened by the surface charges which vary with the wave vector \mathbf{q} .

Consider the z-component of the electric field at $\mathbf{r}_{\perp} = 0$. At this symmetry point the field has no (x, y) -plane

components. The field created by the charge in the gap has the form

$$\begin{aligned}
E_z^{\text{ch}}(z) &= \frac{\rho_0}{4\pi\epsilon_0\epsilon} \int_0^{2\pi} d\varphi \int_0^\infty r_\perp dr_\perp \int_{-d/2}^{d/2} d\tilde{z} \times \\
&\times \frac{\cos(qr_\perp \cos(\varphi))(z - \tilde{z})e^{-\Delta\kappa\tilde{z}}}{(r_\perp^2 + (z - \tilde{z})^2)^{3/2}} = \\
&= \frac{\rho_0}{2\epsilon_0\epsilon} \left\{ \frac{e^{-qz}}{q - \Delta\kappa} (e^{(q-\Delta\kappa)z} - e^{-(q-\Delta\kappa)d/2}) + \right. \\
&\left. + \frac{e^{qz}}{q + \Delta\kappa} (e^{-(q+\Delta\kappa)d/2} - e^{-(q+\Delta\kappa)z}) \right\}. \tag{A6}
\end{aligned}$$

The electric field created by the surface metal charges is given by the expression

$$E_z^{\text{m}}(z) = \frac{\rho_0}{2\epsilon_0\epsilon} (\sigma_2 e^{-q(z+d/2)} + \sigma_1 e^{q(z-d/2)}), \tag{A7}$$

where the surface charges $\sigma_{1,2}$ are

$$\sigma_{1(2)} = \frac{\sigma_{1(2)}^0 e^{qd} + \sigma_{2(1)}^0}{e^{qd} - e^{-qd}}, \tag{A8}$$

with

$$\begin{aligned}
\sigma_1^0 &= \frac{e^{-qd/2}}{q - \Delta\kappa} \left(e^{(q-\Delta\kappa)d/2} - e^{-(q-\Delta\kappa)d/2} \right), \\
\sigma_2^0 &= \frac{e^{-qd/2}}{q + \Delta\kappa} \left(e^{-(q+\Delta\kappa)d/2} - e^{(q+\Delta\kappa)d/2} \right). \tag{A9}
\end{aligned}$$

The total value of the z-component of electric field due to the charge $\rho^{(1)}$ is the sum, $E_z^{(1)} = E_z^{\text{ch}} + E_z^{\text{m}}$. Similarly we can calculate the amplitude of the in-plane field component $E_x^{(1)}$. Its spatial variation is shifted by a half period $1/(2q)$.

Both charges in Eq. (A4) have the same period of oscillations and the same phase. The field produced by the charge $\rho^{(2)}$ is the same as the field $\mathbf{E}^{(1)}$, ($E_z^{(2)}(z) = E_z^{(1)}(z)$), ($E_x^{(2)}(z) = E_x^{(1)}(z)$). The surface density (density per surface area of leads) of interaction energy can be calculated as follows $W_I = (\epsilon_0\epsilon/2) (\int dz E_z^{(1)}(z) E_z^{(1)}(z) + \int dz E_x^{(1)}(z) E_x^{(1)}(z))$, where integration goes over the region $|z| < d/2$. Finally, the matrix element can be estimated as follows

$$W_I = W_{I_x} + W_{I_z}, \tag{A10}$$

where

$$\begin{aligned}
W_{I_z} &= \frac{\rho_0^2}{8\epsilon_0\epsilon} \left\{ (\alpha_1^2 + \alpha_2^2) \frac{\sinh(dq)}{q} + \alpha_3^2 \frac{\sinh(d\Delta\kappa)}{q} \right. \\
&\quad + 2\alpha_1\alpha_2 d + 4\alpha_1\alpha_3 \frac{\sinh((\Delta\kappa + q)d/2)}{\Delta\kappa + q} \\
&\quad \left. + 4\alpha_2\alpha_3 \frac{\sinh((\Delta\kappa - q)d/2)}{\Delta\kappa - q} \right\}, \\
W_{I_x} &= \frac{\rho_0^2}{8\epsilon_0\epsilon} \left\{ (\tilde{\alpha}_1^2 + \tilde{\alpha}_2^2) \frac{\sinh(dq)}{q} + \tilde{\alpha}_3^2 \frac{\sinh(d\Delta\kappa)}{q} \right. \\
&\quad + 2\tilde{\alpha}_1\tilde{\alpha}_2 d + 4\tilde{\alpha}_1\tilde{\alpha}_3 \frac{\sinh((\Delta\kappa + q)d/2)}{\Delta\kappa + q} \\
&\quad \left. + 4\tilde{\alpha}_2\tilde{\alpha}_3 \frac{\sinh((\Delta\kappa - q)d/2)}{\Delta\kappa - q} \right\}, \tag{A11}
\end{aligned}$$

with

$$\alpha_1 = e^{-qd/2} \sigma_2 - \frac{e^{-(q-\Delta\kappa)d/2}}{q - \Delta\kappa}, \tag{A12}$$

$$\tilde{\alpha}_1 = -e^{-qd/2} \sigma_2 - \frac{e^{-(q-\Delta\kappa)d/2}}{q - \Delta\kappa}, \tag{A13}$$

$$\alpha_2 = e^{-qd/2} \sigma_1 + \frac{e^{-(q+\Delta\kappa)d/2}}{q + \Delta\kappa}, \tag{A14}$$

$$\tilde{\alpha}_2 = e^{-qd/2} \sigma_1 - \frac{e^{-(q+\Delta\kappa)d/2}}{q + \Delta\kappa}, \tag{A15}$$

$$\alpha_3 = \frac{2\Delta\kappa}{q^2 - \Delta\kappa^2}, \quad \tilde{\alpha}_3 = \frac{-2q}{q^2 - \Delta\kappa^2}. \tag{A16}$$

Introducing W_I into Eq. (A4) we arrive to the final expression for \tilde{I}_{ex}^-

$$\begin{aligned}
\tilde{I}_{\text{ex}}^- &= -\frac{e^2}{32\pi^4\epsilon_0\epsilon} \int_0^{k_F^-} \int_0^{k_1} dk_1 dk_2 |(\tau_1^-)^* \tau_2^-|^2 e^{-d(\kappa_1^- + \kappa_2^-)} \times \\
&\times \int_0^{k_2^{\text{max}} + k_1^{\text{max}}} q \omega_I(q) dq \int_0^{(k_2^{\text{max}} + k_1^{\text{max}})/2} k \zeta(k, q) dk, \tag{A17}
\end{aligned}$$

where

$$\omega_I(q) = \frac{8\epsilon_0\epsilon W_I(q)}{\rho_0^2}. \tag{A18}$$

We introduced the following functions

$$\zeta = \begin{cases} 0, & (\phi_2 < \phi_3) \text{ or } (\phi_1 < \phi_3), \\ \phi_1 - \phi_3, & \text{otherwise,} \end{cases} \tag{A19}$$

where

$$\phi_1(k, q) = \begin{cases} 0, & k > k_1^{\text{max}} + q/2, \\ \frac{\pi + \pi \text{sign}(k_1^{\text{max}} - q/2)}{2}, & k < |k_1^{\text{max}} - q/2|, \\ \arccos\left(\frac{k^2 + q^2/4 - (k_1^{\text{max}})^2}{qk}\right), & \text{otherwise.} \end{cases} \tag{A20}$$

$$\phi_2(k, q) = \begin{cases} \pi, & k < \frac{k_2^{\max} - q/2}{qk}, \\ \arccos\left(\frac{k^2 + q^2/4 - (k_2^{\max})^2}{qk}\right), & \text{otherwise.} \end{cases} \quad (\text{A21})$$

$$\phi_3(k, q) = \pi - \phi_2(k, q). \quad (\text{A22})$$

In a similar way one can calculate the integrals \tilde{I}_{ex}^+ and \tilde{I}_{ex}^- .

-
- ¹ A. D. Kent and D. C. Worledge, *Nature Nanotechnology* **10**, 187 (2015).
- ² C. Chappert, A. Fert, and F. N. V. Dau, *Nature Materials* **6**, 813 (2007).
- ³ W. H. Butler and A. Gupta, *Nature Materials* **3**, 845 (2015).
- ⁴ G. A. Prinz, *Science* **282**, 1660 (1998).
- ⁵ A. Cho, *Science* **296**, 246 (2002).
- ⁶ K. Ando, S. Fujita, J. Ito, S. Yuasa, Y. Suzuki, Y. Nakatani, T. Miyazaki, and H. Yoda, *J. Appl. Phys.* **115**, 172607 (2014).
- ⁷ M. Julliere, *Phys. Lett.* **54A**, 225 (1975).
- ⁸ J. C. Slonczewski, *Phys. Rev. B* **39**, 6995 (1989).
- ⁹ P. Bruno, *Phys. Rev. B* **52**, 411 (1995).
- ¹⁰ M. Y. Zhuravlev, E. Y. Tsymbal, and A. V. Vedyayev, *Phys. Rev. Lett.* **94**, 026806 (2005).
- ¹¹ J. M. Pruneda, R. Robles, S. Bouarab, J. Ferrer, and A. Vega, *Phys. Rev. B* **65**, 024440 (2001).
- ¹² T. Katayama, S. Yuasa, J. Velev, M. Y. Zhuravlev, S. S. Jaswal, and E. Y. Tsymbal, *Appl. Phys. Lett.* **89**, 112503 (2006).
- ¹³ P. M. Haney, C. Heiliger, and M. D. Stiles, *Phys. Rev. B* **79**, 054405 (2009).
- ¹⁴ J. P. Velev, M. Y. Zhuravlev, K. D. Belashchenko, S. S. Jaswal, E. Y. Tsymbal, T. Katayama, and S. Yuasa, *IEEE Transactions on Magnetics* **43**, 2770 (2007).
- ¹⁵ M. Y. Zhuravlev, A. V. Vedyayev, and E. Y. Tsymbal, *J. Phys.: Condens. Matter* **22**, 352203 (2010).
- ¹⁶ R. R. Gareev, D. E. Burgler, M. Buchmeier, R. Schreiber, and P. Grunberg, *Appl. Phys. Lett.* **81**, 1264 (2002).
- ¹⁷ R. R. Gareev, L. L. Pohlmann, S. Stein, D. E. Burgler, and P. A. G. an M. Siegel, *J. Appl. Phys.* **93**, 8038 (2003).
- ¹⁸ J. Faure-Vincent, C. Tiusan, C. Bellouard, E. Popova, M. Hehn, F. Montaigne, and A. Schuhl, *Phys. Rev. Lett.* **89**, 107206 (2002).
- ¹⁹ P. A. A. van der Heijden, P. J. H. Bloemen, J. M. Metseelaar, R. M. Wolf, J. M. Gaines, J. T. W. M. van Eemeren, P. J. van der Zaag, and W. J. M. de Jonge, *Phys. Rev. B* **55**, 11569 (1997).
- ²⁰ H. Yanagihara, Y. Toyoda, and E. Kita, *J. Appl. Phys.* **101**, 09D101 (2007).
- ²¹ W. Skowronski, T. Stobiecki, J. Wrona, K. Rott, A. Thomas, G. Reiss, and S. van Dijken, *J. Appl. Phys.* **107**, 093917 (2010).
- ²² A. Koziol-Rachwal, T. Slezak, M. Slezak, K. Matlak, E. Mlynczak, N. Spiridis, and J. Korecki, *J. Appl. Phys.* **115**, 104301 (2014).
- ²³ C. H. Marrows, N. Wiser, B. J. Hickey, T. P. A. Hase, and B. Tanner, *J. Phys.: Condens. Mat.* **11**, 81 (1999).
- ²⁴ J. C. S. Kools, *J. Appl. Phys.* **77**, 2993 (1999).
- ²⁵ M. Zhuravlev, J. Velev, A. Vedyayev, and E. Tsymbal, *J. Magn. Magn. Mater.* **300**, 277 (2006).
- ²⁶ S. V. Vonsovskii, *Magnetism* (Wiley, New York, 1974) p. 1034.
- ²⁷ L. D. Landau and E. M. Lifshitz, *Quantum Mechanics Nonrelativistic Theory, Course of Theoretical Physics*, 3rd ed., Vol. 3 (Nauka, Moscow, 1976).
- ²⁸ W. Eerenstein, N. D. Mathur, and J. F. Scott, *Nature* **442**, 759 (2006).
- ²⁹ R. Ramesh and N. A. Spaldin, *Nature Mat.* **6**, 21 (2007).
- ³⁰ O. G. Udalov and I. S. Beloborodov, arXiv:1606.02622v1 (2016).
- ³¹ The operator does not include the factor 1/2 because we sum over the equal elements $(U_{ijkl}^{s_1 s_2} \hat{a}_i^{s_1+} \hat{a}_j^{s_2} \hat{b}_k^{s_2+} \hat{b}_l^{s_1})$ and $(U_{jikl}^{s_1 s_2} \hat{a}_k^{s_2+} \hat{a}_i^{s_1} \hat{b}_i^{s_1+} \hat{b}_j^{s_2})$.
- ³² I. L. Aleiner, P. W. Brouwer, and L. I. Glazman, *Phys. Rep.* **358**, 309 (2002).
- ³³ H. Okamoto, T. Mitani, Y. Tokura, S. Koshihara, T. Komatsu, Y. Iwasa, T. Koda, and G. Saito, *Phys. Rev. B* **43**, 8224 (1991).
- ³⁴ K. Kobayashi, S. Horiuchi, R. Kumai, F. Kagawa, Y. Murakami, and Y. Tokura, *Phys. Rev. Lett.* **108**, 237601 (2012).
- ³⁵ J. Muller, T. S. Boscke, U. Schroder, S. Mueller, D. Brauhuis, U. Bottger, L. Frey, and T. Mikolajick, *Nano Letters* **12**, 4318 (2012).
- ³⁶ M. Huth, A. Rippert, R. Sachser, and L. Keller, *Mater. Res. Expr.* **1**, 046303 (2014).
- ³⁷ M. Huth, F. Kolb, and H. Plank, *Appl. Phys. A* **117**, 1689 (2014).
- ³⁸ O. G. Udalov, N. M. Chtchelkatchev, and I. S. Beloborodov, *Phys. Rev. B* **89**, 174203 (2014).
- ³⁹ O. G. Udalov, N. M. Chtchelkatchev, and I. S. Beloborodov, *J. Phys.: Condens. Matter* **27**, 186001 (2015).
- ⁴⁰ O. G. Udalov, N. M. Chtchelkatchev, and I. S. Beloborodov, *Phys. Rev. B* **92**, 045406 (2015).
- ⁴¹ A. M. Belemuk, O. G. Udalov, N. M. Chtchelkatchev, and I. S. Beloborodov, *J. Phys.: Condens. Matter* **28**, 126001 (2016).
- ⁴² V. M. Fridkin, *Phys. Usp.* **49**, 193 (2006).
- ⁴³ V. M. Fridkin, R. V. Gaynutdinov, and S. Ducharme, *Phys. Usp.* **53**, 199 (2010).
- ⁴⁴ J. P. Perdew and A. Zunger, *Phys. Rev. B* **23**, 5048 (1981).
- ⁴⁵ O. Gunnarsson and B. I. Lundqvist, *Phys. Rev. B* **13**, 4274 (1976).